13th ewtec 2019 Proceedings of the 13th European Wave and Tidal Energy Conference 1-6 Sept 2019, Naples, Italy

# An upgraded model for the design of spar-type floating oscillating water column devices

Rui P. F. Gomes, João C. C. Henriques, Luís M. C. Gato, and António F. O. Falcão

***Abstract*—This paper addresses the hydrodynamic optimization of a floating oscillating water column (OWC) wave energy converter. The device, with an axisymmetric geometry and a draft much larger than the horizontal dimension, is known as the OWC spar buoy device. The design of the converter geometry, mass distribution and turbine damping is carried out through the application of a gradient-free optimization algorithm. The algorithm maximizes the annual-averaged power absorbed from a site off the western coast of Portugal. The floating structure is assumed to oscillate in six degrees of freedom and the inner OWC is modelled as a heaving flat surface. Hydrodynamic coefficients are calculated using a boundary integral equation method. The system dynamics is modelled in the frequency domain and irregular-wave sea states power absorption is determined using a stochastic approach. Drag forces due to real fluid effects are taken into account. The optimization method is divided in two different sub-problems to reduce the overall computational time: (i) main optimization; and (ii) internal optimization. The internal optimization problem is used to optimize the turbine and mass distribution parameters. This sub-problem is part of the main optimization problem, which is dedicated to optimizing the geometry. The results present optimized OWC spar buoy geometries and corresponding power output values, for three different drafts. Results suggest that devices with longer draft absorb more energy and are less prone to the undesirable occurrence of parametric resonance.**

***Index Terms*—Wave energy, floating oscillating water column, spar buoy, numerical modelling, optimization algorithm, parametric resonance.**

## I. Introduction

The design of wave energy converters aims the efficient extraction of energy from the ocean waves. However, this is not the only condition, as these devices need to survive long periods of time while subject to severe sea conditions and produce energy at low cost. The necessity of addressing simultaneously different design objectives while dealing with a variety of parameters with significant importance make this matter a complex design problem. Optimization algorithms are an option to overcome these issues.

The geometry optimization of WECs, specially to tune device hydrodynamic response to the incoming wave conditions, using optimization algorithms has been addressed in several studies [1]–[6]. The SEAREV, a floating WEC with an internal pendulum, was optimized using genetic algorithms [1], [2]. The shape optimization of a generic floating WEC, moving essentially in pitch, is reported in [3]. The geometry optimization and power take-off characteristics of the IPS, a heaving two-body WEC, is presented in [4]. An optimization study on the geometrical optimization of an axisymmetric floating oscillating water column (OWC) device is described in [5], which includes the performance comparison between the use of a genetic algorithm and a direct search algorithm. Ref. [7] presents the geometry, mass distribution and PTO optimization of a floating WEC with an internal U-shaped OWC. The shape optimization, using a genetic algorithm, of a submerged planar pressure differential WEC subjected to directional waves can be found in [6]. These studies have shown the effectiveness of optimization algorithms in the improvement of power conversion efficiency.

This paper is focussed on the OWC spar buoy device, a floating oscillating water column with an axisymmetric geometry, with a draft much larger than its diameter. The device consists of a buoy with a tail tube opened at the bottom to the sea water, where the OWC moves. The OWC induces volume variations on an air chamber, forcing an airflow to pass through a turbine. This concept was initially developed by the Japanese naval commander Yoshio Masura for application in navigational buoys [8]. The first known theoretical model developed to assess the device dynamics was reported by McCormick [9]. Whittaker and McPeake [10] carried out experimental tests and developed a two degree of freedom model to evaluate the power output. The hydrodynamic characterization of the device and evaluation of interaction between the floating structure and OWC using boundary element methods can be found in [11]. The detailed optimization of the device geometry for a real wave climate was reported in [5]. The model assumed that only heave was relevant for the energy extraction and neglected the other oscillation modes. Tests of a small-scale model in a wave flume are described in [12], [13]. In [12] the model displacements are limited only to heave, whereas in [13] the model is moored to the flume floor through a

This paper, with ID 1438, has been submitted in the EWTEC 2019 conference track *Wave device development and testing*. This work was supported in part by the Portuguese Foundation for Science and Technology (FCT), through IDMEC, under LAETA, project UID/EMS/50022/2019 and by the European Commission's Horizon 2020 program, project WETFEET, under grant No. 641334. R. P. F. Gomes was supported by post-doctoral fellowship SFRH/BPD/93209/2013 from FCT. J. C. C. Henriques was supported by FCT researcher grant No. IF/01457/2014.

R. P. F. Gomes, J. C. C. Henriques, L. M. C. Gato, and A. F. O. Falcão are with IDMEC, Instituto Superior Técnico, Universidade de Lisboa, Av. Rovisco Pais, 1049-001 Lisboa, Portugal (e-mails: ruigomes@tecnico.ulisboa.pt, joaochenriques@tecnico.ulisboa.pt, luis.gato@tecnico.ulisboa.pt, antonio.falcao@tecnico.ulisboa.pt).

  

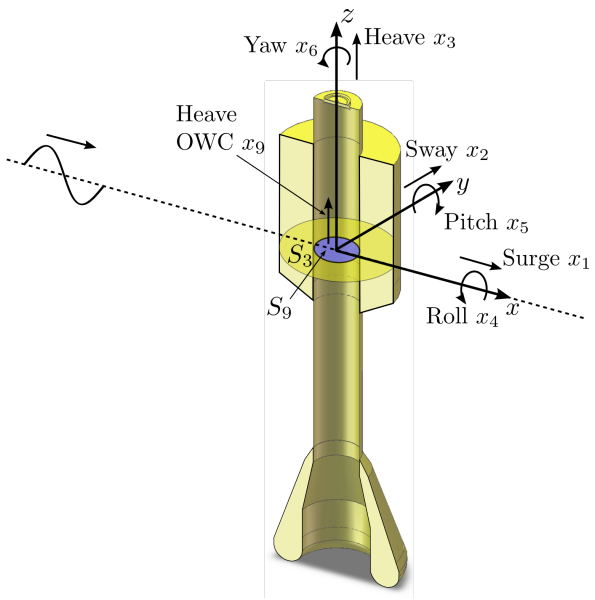


Figure 1. Cut section view of a single OWC spar buoy with indication of the fixed reference frame and oscillation modes.

slack-mooring system.

A previous optimization work on the OWC spar buoy considered only the buoy and OWC heave modes to assess power extraction. However, experimental results (see e.g. [13]) showed that under wave certain conditions, the device can be subject to a dynamic instability that reduces the power output. This effect, known as parametric resonance can occur due to instantaneous variations of hydrostatic restoring moment, or due to nonlinear pressure variations induced by the wave on the instantaneous converter wetted surface. During the wave cycle the device can become unstable, engaging in high roll/pitch amplitudes and consequently reducing power extraction [13]. Parametric resonance can only be computed by a nonlinear model capable of evaluating the instantaneous pressure forces on the hull, which involves a high computational cost (see e.g. [14], [15]). However, the susceptibility of occurrence of this effect can be detected in a simpler way, thought a linear analysis of the device dynamics (see e.g. [13]).

In this paper we present an improved optimization method based on the work presented in [5]. In this case, we evaluate the device dynamics in surge, heave and pitch and implement a penalty on the objective function to account for the power reduction when parametric resonance occurs. Drag forces due to viscous flow effects are also considered. The modelling of the OWC spar buoy is detailed in Section II, which includes the frequency domain and the stochastic approach formulations to evaluate the annual-averaged power output. The optimization method is described in Section III. Section IV presents the numerical optimization results. Relevant conclusions are shown in Section V.

## II. Modelling of the OWC spar buoy

### A. Regular waves

The formulation presented here considers irrotational flow. Linear water wave theory and linear hydrodynamic interactions are considered by assuming that wave amplitude and body motions are small. Fig. 1 presents a cut section view of a single OWC spar buoy with the indication of the fixed reference frame used for the mathematical formulation. The waterplane area of the buoy $S_3$ and of the OWC $S_9$ are indicated in the figure. Due to system symmetry, the model considers four oscillation modes, three for the floating structure (buoy) (surge $x_1$, heave $x_3$, pitch $x_5$) and one for the internal free surface (heave $x_9$). The internal free surface is modelled as a rigid piston with a small thickness, as in [5]. The time-dependent coordinates of the buoy and OWC displacement are $x_1(t)$, $x_3(t)$, $x_5(t)$ and $x_9(t)$, where $t$ is time. All are zero at equilibrium and increase in the direction of the corresponding axes. The model interacts with two-dimensional regular waves with amplitude $A_\mathrm{w}$ and angular frequency $\omega$, travelling with the $x$-axis direction. The equation of motion for each oscillating mode ($i, j = 1, 3, 5, 9$) in the time domain is

$$\sum_j M_{ij}\ddot{x}_j = f_{\mathrm{e},i} + f_{\mathrm{r},i} + f_{\mathrm{h},i} + f_{\mathrm{t},i} + f_{\mathrm{d},i} + f_{\mathrm{m},i}\,, \qquad (1)$$

where $M_{ij}$ represents the inertia coefficients of the system, $f_{\mathrm{e},i}$ is the wave excitation force, $f_{\mathrm{r},i}$ is the wave radiation force, $f_{\mathrm{h},i}$ is the hydrostatic force, $f_{\mathrm{t},i}$ is the force due to the air chamber pressure variations, $f_{\mathrm{d},i}$ is the drag force due to viscous effects and $f_{\mathrm{m},i}$ is the mooring force. The symbol dot represents a time derivative.

The air chamber volume variation over time produces pressure oscillations that force the passage of air thought the turbine. Considering a positive value for outward flow, the mass flow rate through the turbine is $\dot{m}_t = -d(\varrho_\mathrm{a}V)/dt$, where $V(t)$ is the instantaneous air chamber volume and $\varrho_\mathrm{a}$ is the air density. By assuming air as an ideal gas and the air volume compression/expansion cycles as isentropic processes, as proposed in [16], $\dot{m}_t$ can be approximated as proportional to the relative velocity between the heave modes (buoy and OWC) and to the time-derivative of the pressure difference between the air chamber and the atmosphere,

$$\dot{m}_\mathrm{t} = -\varrho_\mathrm{a} S_9\,(\dot{x}_3 - \dot{x}_9) + \frac{V_0}{c_\mathrm{a}^2}\frac{dp}{dt}\,, \qquad (2)$$

where $V_0$ is the volume of the air chamber in still water conditions and $c_\mathrm{a}$ is the speed of sound in air. As a simplification, $V_0$ is assumed to be much larger than the air chamber volume variations $S_9(x_3 - x_9)$, while $c_\mathrm{a}$ and $\varrho_\mathrm{a}$ are assumed to be constant and equal to their values under atmospheric conditions. This isentropic linearized relationship provides a good approximation for the air chamber dynamics if the system is not subject to extreme sea conditions [17].

In this work, a turbine with a linear characteristic curve is considered, i.e., the turbine presents a proportional relationship between the flow rate and the pressure difference,

$$\dot{m}_\mathrm{t}(t) = k_\mathrm{t}\,p(t)\,, \qquad (3)$$

where $k_\mathrm{t}$ is the linear (constant) turbine coefficient, which depends on the turbine size and rotational

speed. The Wells turbine, widely used in OWC devices, presents this type of relationship.

Since all the forces are assumed to be linear and the system is subject to a regular-wave excitation, it is possible to express the time-dependent quantities as

$$\begin{aligned}\{x_i, \dot{x}_i, \ddot{x}_i, p\ , f_{\mathrm{e},i}, f_{\mathrm{r},i}, f_{\mathrm{h},i}, f_{\mathrm{t},i}, f_{\mathrm{d},i}, f_{\mathrm{m},i}\}(t) = \\ \mathrm{Re}\left(\{X_i, \mathbf{i}\omega X_i, -\omega^2 X_i, \mathcal{P}, \right. \\ \left. F_{\mathrm{e},i}, F_{\mathrm{r},i}, F_{\mathrm{h},i}, F_{\mathrm{t},i}, F_{\mathrm{d},i}, F_{\mathrm{m},i}\} \exp(\mathbf{i}\omega t)\right)\ ,\end{aligned} \tag{4}$$

where $\mathbf{i}$ is the imaginary unit and $\omega$ is the incoming wave frequency. The amplitudes $X_i$, $\mathcal{P}$ , $F_{\mathrm{e},i}$, $F_{\mathrm{r},i}$, $F_{\mathrm{h},i}$, $F_{\mathrm{t},i}$, $F_{\mathrm{d},i}$, $F_{\mathrm{m},i}$ are complex quantities. The equation of motion in the frequency domain becomes

$$\sum_j -\omega^2 M_{ij} X_j = F_{\mathrm{e},i} + F_{\mathrm{r},i} + F_{\mathrm{h},i} + F_{\mathrm{t},i} + F_{\mathrm{d},i} + F_{\mathrm{m},i}\ , \tag{5}$$

where $X_j$ represent the complex amplitude of the oscillation mode ($j = 1$ for the buoy's surge, $j = 3$ for the buoy's heave, $j = 5$ for the buoy's pitch and $j = 9$ for the OWC's heave). Note that the motion of the system at any given instant $t$ is $x_i(t) = \mathrm{Re}(X_i e^{\mathbf{i}\omega t})$. The forces acting on the right-hand-side of (5) are presented in the following subsections.

*1) Hydrodynamic forces:* The complex amplitude of the wave excitation force, due to the action of the waves on the device, is

$$F_{\mathrm{e},i} = A_{\mathrm{w}} \Gamma_i\ , \tag{6}$$

where $\Gamma_i$ the excitation force coefficient of mode $i$. The radiation force, caused by wave radiation due to the device motion, is

$$F_{\mathrm{r},i} = \sum_j \left(\omega^2 A_{\mathrm{r},ij} - \mathbf{i}\omega B_{\mathrm{r},ij}\right) X_j\ , \tag{7}$$

where $A_{\mathrm{r},ij}$ represents the added inertia coefficient and $B_{\mathrm{r},ij}$ the radiation damping coefficient.

The linear hydrodynamic coefficients ($A_{\mathrm{r},ij}$, $B_{\mathrm{r},ij}$ and $\Gamma_i$) were computed using a boundary integral equation method (BIEM) [18]. The higher-order discretization method was used. More information on this modelling can be found in [5].

*2) Hydrostatic force:* The hydrostatic force acting on the device oscillating mode $i$ is

$$F_{\mathrm{h},i} = \sum_j C_{\mathrm{h},ij} X_j\ , \tag{8}$$

where $C_{\mathrm{h},ij}$ is the linear hydrostatic coefficient. In this case, the non-zero terms are

$$\begin{aligned} C_{\mathrm{h},33} &= \varrho_{\mathrm{w}} g S_3\ , \\ C_{\mathrm{h},55} &= \varrho_{\mathrm{w}} g \mathcal{V} \overline{GM}\ , \\ C_{\mathrm{h},99} &= \varrho_{\mathrm{w}} g S_9\ , \end{aligned} \tag{9}$$

where $\varrho_{\mathrm{w}}$ is the water density, $g$ is the acceleration of gravity, $S_3$ is the buoy waterplane area, $S_9$ is the OWC inner free surface area, $\mathcal{V}$ is the buoy displaced volume and $\overline{GM}$ is the buoy metacentric height.

*3) Force due to air pressure variations:* The air pressure variation inside the OWC air chamber affects the heave motion of the buoy and of the OWC. The forces being applied on these oscillating modes due to the air chamber pressure variations are

$$\begin{aligned} F_{\mathrm{t},3} &= S_9 \mathcal{P}\ , \\ F_{\mathrm{t},9} &= -S_9 \mathcal{P}\ , \end{aligned} \tag{10}$$

where $\mathcal{P}$ is the complex amplitude of the pressure difference between the air chamber and the exterior atmosphere. This parameter is determined by solving (2)-(3) in the frequency domain,

$$\mathcal{P} = -\frac{\mathbf{i}\dfrac{\omega \varrho_{\mathrm{a}} S_9}{k_{\mathrm{t}}} + \dfrac{\omega^2 \varrho_{\mathrm{a}} S_9 V_0}{c_{\mathrm{a}}^2 k_{\mathrm{t}}^2}}{1 + \left(\dfrac{\omega V_0}{k_{\mathrm{t}} c_{\mathrm{a}}^2}\right)^2} (X_3 - X_9)\ . \tag{11}$$

This equation shows the linear relation between the relative heave displacement between the buoy and the OWC and the pressure difference. The imaginary term is related with the damping effect from the air turbine power extraction, whereas the real term is associated with the spring-like effect due to the compressibility of air inside the chamber.

The power available to the air turbine is computed using the pressure difference complex amplitude. The time-averaged power available to the turbine over a regular-wave wave cycle is

$$\overline{P}_t = \frac{k_{\mathrm{t}}}{2\varrho_{\mathrm{a}}} |\mathcal{P}|^2\ . \tag{12}$$

*4) Mooring force:* The mooring system produces a restoring effect to keep the device on station. The mooring force complex amplitude is

$$F_{\mathrm{m},i} = C_{\mathrm{m},i} X_i\ , \tag{13}$$

where $C_{\mathrm{m},i}$ is the mooring restoring coefficient. In this case, we assume that the moorings only affect surge. The corresponding restoring coefficient $C_{\mathrm{m},1}$ is determined from the specified surge natural period $T_{n1,\mathrm{spc}}$, normally much larger than the usual wave periods,

$$C_{\mathrm{m},1} = \omega_{n1,\mathrm{spc}}^2 \left(m_1 + A_{\mathrm{r},11}\left(\omega_{n1,\mathrm{spc}}\right)\right)\ , \tag{14}$$

where $m_1$ is the device mass ($m_1 = \varrho_{\mathrm{w}} \mathcal{V}$) and $\omega_{n1,\mathrm{spc}} = 2\pi / T_{n1,\mathrm{spc}}$.

### *B. Irregular waves*

The dynamics and energy extraction of the OWC spar buoy OWC under irregular waves is computed using a stochastic method, as in [12], [19]. This approach uses the linear response amplitude operators computed by the model from Section 1 to determine statistically representative values of the device dynamics and power extraction. We consider a random sea state represented by the superposition of elementary regular wave components with amplitude $A_{\mathrm{w}}$ and frequency $\omega$. The free-surface elevation $\eta$ is considered to be stationary, ergodic and a Gaussian process [20]. The probability density function of the free-surface elevation is

$$f_{\mathrm{pdf}}(\eta) = \frac{1}{\sqrt{2\pi}\sigma_\eta} \exp\left(-\frac{\eta^2}{2\sigma_\eta^2}\right)\ , \tag{15}$$

where $\sigma_\eta$ is the standard deviation of $\eta$,

$$\sigma_\eta^2 = \int_0^\infty S_\omega(\omega)\, \mathrm{d}\omega\ , \tag{16}$$

where $S_\omega$ is the random sea state energy density spectrum,

$$S_\omega(\omega) = \frac{A_{\mathrm{w}}^2(\omega)}{2\Delta\omega}, \tag{17}$$

where $A_{\mathrm{w}}$ is the wave amplitude of a wave component and $\Delta\omega$ is the frequency interval of the discretization of $S_\omega$.

The system presents a linear response and $\eta$ is described by a Gaussian probability density function, therefore any variable $\chi$ with a linear response, i.e. proportional to $A_{\mathrm{w}}$, can also be described by a Gaussian probability density function. The standard deviation of the system response $\chi$ ($\sigma_\chi$) is

$$\sigma_\chi^2 = \int_0^\infty S_\omega(\omega) \left| \frac{\mathcal{X}(\omega)}{A_{\mathrm{w}}} \right|^2 \mathrm{d}\omega, \tag{18}$$

where $\chi(t) = \mathrm{Re}(\mathcal{X} e^{\mathbf{i}\omega t})$.

For a given sea state represented by an energy density spectrum $S_\omega$, the time-averaged power available to the turbine is

$$\overline{P}_{\mathrm{t,irr}} = \frac{k_{\mathrm{t}}}{\varrho_{\mathrm{a}}} \sigma_p^2, \tag{19}$$

where $\sigma_p$ is the standard deviation of the pressure difference $p$, which is computed through (18).

The annual-averaged power available to the turbine $\overline{P}_{\mathrm{t,ann}}$ is computed by considering the power extracted from the different sea states representative of the wave climate under consideration. For a wave climate consisting of $N$ different sea states, the annual-averaged power available to the turbine is

$$\overline{P}_{\mathrm{t,ann}} = \sum_{n=1}^{N} \phi_n \overline{P}_{\mathrm{t,irr},n}, \tag{20}$$

where $\phi_n$ is the probability of occurrence of the $n$-th sea state.

### C. Linearisation of drag forces

The drag forces, caused by viscous flow effects, are modelled as being proportional to the square of the relative flow velocity on the device, similarly to the drag term in Morison's equation [21]. Since we are using a linear model to evaluate the device dynamics, the linearization of these forces is required.

To compute the horizontal drag forces acting on the device, we take advantage of the device axisymmetric geometry and consider the two-dimensional case of the drag induced by a uniform flow past a circular cylinder. At a given horizontal section with vertical coordinate $z$, the complex amplitude of the $x$-axis velocity components of the relative flow between the buoy and the wave particles is

$$U_{\mathrm{r},x}(\omega, z) = \mathbf{i}\omega X_1(\omega) + \mathbf{i}\omega X_5(\omega) z - U_{\mathrm{w},x}(\omega, z), \tag{21}$$

where $\mathbf{i}\omega X_1$ is the complex amplitude of surge velocity, $\mathbf{i}\omega X_5$ is the complex amplitude of pitch angular velocity, and $U_{\mathrm{w},x}$ is the $x$-axis component of the complex amplitude of the wave particles velocity [22].

For the linearization of the drag forces, we adopted the method suggested in [20], which linearizes the drag forces using the standard deviation of the oscillatory velocity for a given sea state. This approach considers that a given oscillatory velocity $u$ follows a Gaussian probability distribution with mean zero and standard deviation $\sigma_u$. The minimization of the difference between the quadratic force (proportional to $|u|u$) and the linear approximation shows that $|u|u \approx \sqrt{8/\pi}\sigma_u u$. Here, the slender structure is discretized into a finite number of horizontal circular sections, each with a given diameter. The force acting in surge ($F_{\mathrm{d},1}$) and the moment acting in pitch ($F_{\mathrm{d},5}$) are computed through the numerical integration over the $z$-axis direction. The force on each section with depends on the drag coefficient of an uniform flow past a two-dimensional cylinder ($c_{\mathrm{d,cyl}}$) and on the standard deviation of the relative horizontal velocity for each vertical position ($\sigma_{u_{\mathrm{r},x}}(z)$), which depends on the sea state. The relative horizontal velocity is $u_{\mathrm{r},x}(t) = \mathrm{Re}(U_{\mathrm{r},x} e^{\mathbf{i}\omega t})$.

For the drag force being applied on the heave modes (buoy and OWC), we adopt the model presented in [12]. Two sources of drag forces are considered. One drag force is proportional to the relative velocity between the buoy and the water particles $z$-axis component ($\mathbf{i}\omega X_3 - U_{\mathrm{w},z}$) at the same vertical level as the drag-inducing surface. These surfaces are the bottom surface of the floater and bottom surface of the OWC tube. The second force is proportional to the relative velocity between the buoy and the OWC ($\mathbf{i}\omega X_3 - \mathbf{i}\omega X_9$). As indicated in [12], the drag force applied on the buoy heave mode ($F_{\mathrm{d},3}$) depends on the drag coefficient of the drag-inducing surfaces of the buoy $c_{\mathrm{d},3}$, on the drag coefficient of the tube $c_{\mathrm{d},39}$, on the standard deviation of the relative velocity between the buoy heave and the vertical motion of the wave particles $\sigma_{(\dot{x}_3 - u_{\mathrm{w},z})}$, and on the standard deviation of the relative heave velocity between the buoy and the OWC $\sigma_{(\dot{x}_3 - \dot{x}_9)}$. In the case of the OWC heave mode, $F_{\mathrm{d},9}$ depends on $c_{\mathrm{d},39}$ and on $\sigma_{(\dot{x}_3 - \dot{x}_9)}$.

The complex amplitudes of the oscillating modes $X_j$ are obtained by solving the system of linear equations describing the motion of the buoy and OWC (see (5)). Since the linerization of the drag forces requires the standard deviation of the system velocities ($\sigma_{u_{\mathrm{r},x}}$, $\sigma_{(\dot{x}_3 - u_{\mathrm{w},z})}$, $\sigma_{(\dot{x}_3 - \dot{x}_9)}$), the system of equations needs to be solved iteratively to reach convergence, updating those values at each step.

## III. Optimization method

The method considered for optimization the OWC spar buoy is focussed on geometrical dimensions but also on turbine and mass distribution parameters, since they are all relevant to the power extraction. Previous studies (see e.g. [1], [4], [5], [7]) have found that a large computational time is spent in the calculation of the hydrodynamic coefficients, when a boundary integral equations method (BIEM) is used. Since the linear hydrodynamic coefficients computation is only dependent on geometrical parameters, the optimization problem is commonly divided in two different problems, which reduces the overall computational time. Here, we decided to divide the optimization problem in: (i) main optimization problem; and (ii) internal optimization problem. The internal optimization problem

is used exclusively to optimized the turbine and mass distribution parameters for a given converter geometry. This problem is part of the main optimization problem, which is only dedicated to solving the geometrical problem. Therefore, for each converter geometry, the internal optimization guarantees that the optimal turbine characteristics and mass distribution parameters are applied.

The two optimization problems are solved using the algorithm Constrained Optimization BY Linear Approximations (COBYLA). This method does not require the evaluation of the objective function gradient to obtain convergence. This is an important feature because spurious oscillations of the objective function, due to numerical approximations [4], [5], generate errors in the function gradient evaluation. The optimization algorithm COBYLA is a direct search method that performs linear approximations of the objective function and its constraints [23]. Such approximations are done by the interpolation at the $n+1$ vertices of a simplex (being $n$ the number of variables). At each iteration, the objective function approximation is optimized inside a trust region, while verifying the problem constraints. When the new vertex is better than any of the others vertices of the simplex, the new vertex replaces an existing one. The iterative process continues until no improvement is verified. At that stage, the trust region is reduced to induce contraction of the simplex. Generally, convergence is found when the radius of the trust region reaches a minimum value, which normally defines the accuracy of the solution. Computations were performed in Python using the COBYLA algorithm from the Scipy optimization library.

### *D. Mass distribution considerations*

The OWC spar buoy mass distribution is determined by considering the geometry presented in Fig. 2. The OWC spar buoy geometry consists of a set of 16 surfaces with simple shape (cylindrical, conical, annular, toroidal). We assume that those surfaces represent steel plates, all with the same thickness $t_{\mathrm{stl}}$. Each surface was parametrized and the surface area, mass, centre of mass and moment of inertia were determined. The total steel structure mass $m_{\mathrm{stl}}$, $z$-coordinate of the centre of mass $z_{\mathrm{m,stl}}$ and moment of inertia $I_{55,\mathrm{stl}}$ was determined using the parallel axis theorem.

The device total mass $m_1$ is computed from the displaced volume of water. Therefore, the mass of ballast is given by

$$m_{\mathrm{bal}} = m_1 - m_{\mathrm{stl}}\,, \tag{22}$$

where $m_1 > m_{\mathrm{stl}}$. We consider that the ballast can be located in two vertical positions ($z_{\mathrm{bal1}}$ and $z_{\mathrm{bal2}}$) on the buoy to allow the control of metacentric height, as presented in Fig. 2, therefore $m_{\mathrm{bal}} = m_{\mathrm{bal1}} + m_{\mathrm{bal2}}$. For simplicity, we assume that each ballast is concentrated in a point in the axisymmetric axis. The minimum vertical position of the centre of mass $z_m$ occurs when the ballast is all at the lower position (ballast 1),

$$z_{\mathrm{m,min}} = \frac{z_{\mathrm{m,stl}} m_{\mathrm{stl}} + z_{\mathrm{bal1}} m_{\mathrm{bal}}}{m_1}\,, \tag{23}$$

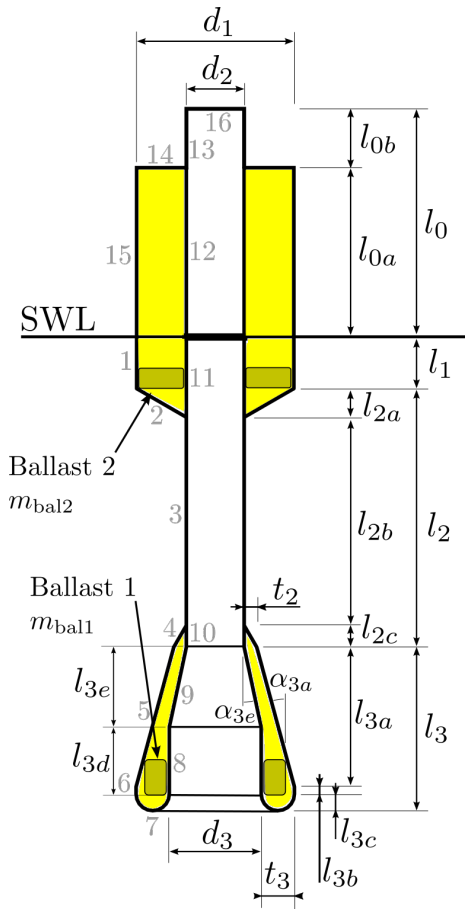


Figure 2. Cut section view of the OWC spar buoy geometry with indication of the relevant dimensions. The numbers indicate the index of each steel surface. The ballast sections in the structure are shown.

therefore, the maximum metacentric height $\overline{GM}_{\max}$ is

$$\overline{GM}_{\max} = \frac{J_{11}}{\mathcal{V}} + z_{\mathrm{b}} - z_{\mathrm{m,min}}\,, \tag{24}$$

where $J_{11}$ is the second moment of area about the $y$-axis of the waterplane area, $\mathcal{V}$ is the displaced water volume ($\mathcal{V} = m_1/\varrho_{\mathrm{w}}$) and $z_{\mathrm{b}}$ is the $z$-coordinate of the centre of buoyancy. The minimum value of the metacentric height $\overline{GM}_{\min}$ should be specified to guarantee stability. Note that, if $\overline{GM}_{\min} > \overline{GM}_{\max}$ the geometry is not feasible since it does not have the minimum stability conditions. Therefore, the geometry should be discarded or a smaller steel thickness should be considered.

For optimization purposes, the device metacentric height is defined as

$$\overline{GM} = c_{\mathrm{m}}\left(\overline{GM}_{\max} - \overline{GM}_{\min}\right) + \overline{GM}_{\min}\,, \tag{25}$$

where $c_{\mathrm{m}}$ is a parameter that can take values between 0 and 1, and is used to control the $\overline{GM}$ within acceptable values ($\overline{GM}_{\min} < \overline{GM} < \overline{GM}_{\max}$). The device's centre of mass $z$-coordinate is

$$z_{\mathrm{m}} = \frac{J_{11}}{\mathcal{V}} + z_{\mathrm{b}} - \overline{GM}\,. \tag{26}$$

Since the $z_{\mathrm{m}}$ is known, it is possible to determine $m_{\mathrm{bal1}}$ and $m_{\mathrm{bal2}}$. The device's moment of inertia is computed through the parallel axis theorem using the masses of

the two ballast sections and the mass and moment of inertia of the steel structure.

### *E. Susceptibility of occurrence of parametric resonance*

Spar-type structures are typically prone to Mathieu instability problems, which results in large undesirable pitch/roll motions [13]. The calculation of this effect require a complex model and a high computational effort due to computation of the instantaneous wetted surface of the floating device [14], [15]. However, the determination of the range of frequencies where this effect occurs may be done through the analysis of linear hydrodynamics.

In this section, we study the susceptibility of occurrence of parametric resonance based on the formulation presented in [13]. The variation of the metacentric height can be determined through the variation of the centre of buoyancy of the floating structure. In its turn, the variation of the centre of buoyancy can be approximately estimated by the amplitude of the heave displacement relative to the vertical displacement of the free surface ($x_3 - \eta$), which measures the amplitude of submergence of the buoy. This estimation can be determined by the linear model presented in the previous sections. The occurrence of parametric resonance can be determined through the analysis of the instability regions of the damped Mathieu equation. For certain wave frequencies, the solution of Mathieu equation is unstable, corresponding in practice to pitch/roll amplitude increasing at a constant rate over time until it reaches a threshold amplitude, where other nonlinear phenomena become dominant (e.g., a significant variation of the waterplane area). A stability diagram ($\delta$ versus $\varepsilon$) can provide the range of wave frequencies and wave amplitudes at which the device can engage in parametric resonance. The limits of stability of the damped Mathieu equation can be determined using a perturbation method [25]. A stability diagram indicate those limits through the plot of $\varepsilon$ as a function of $\delta$. These non-dimensional coefficients are given by

$$\delta = \left(\frac{\omega_{n5}}{\omega}\right)^2 , \tag{27}$$

$$\varepsilon = a_1 \left(\frac{\omega_{n5}}{\omega}\right)^2 , \tag{28}$$

where $a_1$ is the non-dimensional amplitude of the metacentric height variation and $\omega_{n5}$ is the pitch natural frequency, which can be determined through

$$\omega_{n5}^2 = \frac{\varrho_\mathrm{w} g V \overline{GM}_0}{I_{55} + A_{\mathrm{r},55}} . \tag{29}$$

Through the calculation of $a_1$ and $\omega_{n5}$, it is possible to determine the susceptibility of occurrence of parametric resonance by identifying whether the pair of values $(\delta, \varepsilon)$ are inside or outside of the stability region. The effectiveness of this model to determine the occurrence of parametric resonance is shown in [13], using experimental results from a generic geometry of the OWC spar buoy device. In general, parametric resonance occurs in the vicinity of $\omega = 2\omega_{n5}$, and the region tends to expand as the metacentric height amplitude increases (e.g. due to the increase of the wave amplitude). By analysing the stability diagram $\varepsilon$ versus $\delta$, it is possible to calculate the interception points between our case and the transition curves. This allow us to determine the frequency interval $[\omega_\mathrm{i}, \omega_\mathrm{f}]$ were parametric resonance occurs.

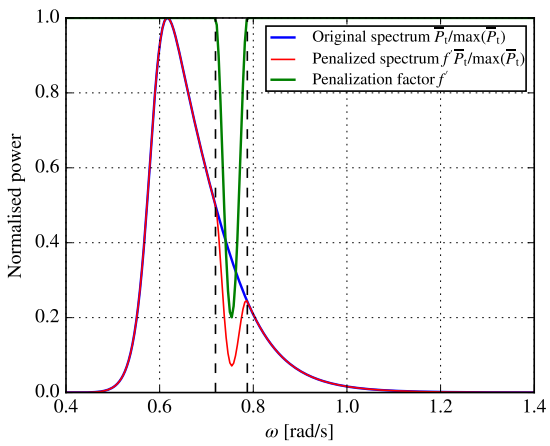


Figure 3. Normalized power spectrum showing the implementation of the penalization factor $f'$ on the power spectrum for the calculation of the penalty function $f_{\mathrm{p,PR}}$. The frequency interval $[\omega_\mathrm{i}, \omega_\mathrm{f}]$ is represented by the dashed vertical lines.

### *F. Objective function*

In this paper, the optimization of the OWC spar buoy addresses the maximization of the annual-averaged power available to the turbine. The objective function $f_\mathrm{obj}$ is affected by three penalty functions used to mitigate large surge and pitch motions, i.e. undesirable motions that could compromise the device structural integrity and mooring system.

The surge penalty function is defined as

$$f_{\mathrm{p},x_1} = 1 - c_\mathrm{pen} \frac{\sigma_{x_1,\mathrm{ann}}}{\sigma_{x_1,\mathrm{ref}}} , \tag{30}$$

and the pitch penalty function is defined as

$$f_{\mathrm{p},x_5} = 1 - c_\mathrm{pen} \frac{\sigma_{x_5,\mathrm{ann}}}{\sigma_{x_5,\mathrm{ref}}} , \tag{31}$$

where $c_\mathrm{pen}$ is a coefficient to control the importance of the penalty functions in the objective function, $\sigma_{x_1,\mathrm{ann}}$ is the annual-averaged standard deviation value of surge (this considers the probability of occurrence of each sea state, $\sigma_{x_1,\mathrm{ann}} = \sum_{n=1}^{N} \phi_n \sigma_{x_1,n}$), $\sigma_{5,\mathrm{ann}}$ is the annual-averaged standard deviation value of pitch ($\sigma_{x_5,\mathrm{ann}} = \sum_{n=1}^{N} \phi_n \sigma_{x_5,n}$), and $\sigma_{x_1,\mathrm{ref}}$ and $\sigma_{x_5,\mathrm{ref}}$ are the reference values for the standard deviation value of surge and pitch, respectively. In this case, we consider $c_\mathrm{pen} = 0.01$, $\sigma_{x_1,\mathrm{ref}} = 1\,\mathrm{m}$ and $\sigma_{x_5,\mathrm{ref}} = 1\,\mathrm{deg}$. If the surge and pitch motions are zero, the penalty functions $f_{\mathrm{p},x_1}$ and $f_{\mathrm{p},x_5}$ have no impact on the objective function, since their values would be 1. If the surge and pitch motions have non-zero values, the penalty functions $f_{\mathrm{p},x_1}$ and $f_{\mathrm{p},x_5}$ would be smaller than 1.

The third penalty function is related with the mitigation of parametric resonance. As discussed before, it is possible to evaluate the interval of frequencies $[\omega_\mathrm{i}, \omega_\mathrm{f}]$ where the device is susceptible to parametric

Table I
PARAMETERS USED IN THE MODELLING OF THE OWC SPAR BUOY DYNAMICS.

| Parameter | Value |
|---|---|
| Water depth $h$ [m] | $\infty$ |
| Water density $\varrho_{\mathrm{w}}$ [kg/m$^3$] | 1025 |
| Acceleration of gravity $g$ [m/s$^2$] | 9.807 |
| Air density $\varrho_{\mathrm{a}}$ [kg/m$^3$] | 1.204 |
| Speed of sound in air $c_{\mathrm{a}}$ [m/s] | 343.3 |
| Steel density $\varrho_{\mathrm{stl}}$ [kg/m$^3$] | 7800 |
| Steel thickness $t_{\mathrm{stl}}$ [m] | 0.015 |
| Drag coefficient in heave $c_{\mathrm{d3}}$ [-] | 0.73 |
| Drag coefficient in OWC tube $c_{\mathrm{d39}}$ [-] | 1.97 |
| Drag coefficient of cylinder $c_{\mathrm{d,cyl}}$ [-] | 2.00 |
| Surge natural period $T_{n1,\mathrm{spc}}$ [s] | 100.0 |
| Minimum metacentric heigh $\overline{GM}_{\min}$ [m] | 3.0 |

Table II
DESIGN PARAMETERS CONSIDERED FOR THE GEOMETRY OPTIMIZATION OF THE OWC SPAR BUOY.

| Design parameter | Initial guess | Lower bound | Upper bound |
|---|---|---|---|
| $l_3/(l_2+l_3)$ | 0.3693 | 0.20 | 0.80 |
| $d_3/d_2$ | 1.4870 | 1.00 | 2.00 |
| $t_2/d_2$ | 0.1993 | 0.10 | 0.50 |
| $t_3/d_2$ | 0.6283 | 0.10 | 0.50 |
| $l_{3a}/(l_{3a}+l_{3b})$ | 0.9500 | 0.05 | 0.95 |
| $l_{3e}/(l_{3e}+l_{3d})$ | 0.5556 | 0.05 | 0.95 |
| $d_2/d_1$ | 0.4015 | 0.20 | 0.80 |

resonance. Since this analysis is done for irregular wave conditions, instead of the amplitude of $x_3-\eta$, we consider the standard deviation of $x_3-\eta$ ($\sigma_{(x_3-\eta)}$) to determine the interceptions with the transition curves in the stability diagram. We start by defining a continuous function $f'$ (penalization factor) over frequency that has the value of 1 outside the interval $[\omega_{\mathrm{i}},\omega_{\mathrm{f}}]$ and has a minimum value in the middle of the frequency interval. This function indicates the relative loss of power over frequency due to parametric resonance. To determine the impact of parametric resonance on the power extraction, the penalization factor is multiplied by the power spectrum. Fig. 3 presents original power spectrum $\overline{P}_{\mathrm{t}}$, the penalization factor $f'$ and the final power spectrum $f'\overline{P}_{\mathrm{t}}$. The penalty function measuring the parametric resonance effect is defined as

$$f_{\mathrm{p,PR}}=\sum_{n=1}^{N}\frac{\int_0^{\infty}(1-f')\,S_{\omega}\dfrac{\overline{P}_{\mathrm{t}}}{A_{\mathrm{w}}^2}\mathrm{d}\omega}{\int_0^{\infty}S_{\omega}\dfrac{\overline{P}_{\mathrm{t}}}{A_{\mathrm{w}}^2}\mathrm{d}\omega}, \tag{32}$$

where $N$ represent the total number of sea states being considered.

Finally, the objective function of the optimization problem is given by

$$f_{\mathrm{obj}}=f_{\mathrm{p},x_1}f_{\mathrm{p},x_5}f_{\mathrm{p,PR}}\frac{\overline{P}_{\mathrm{t,ann}}}{\overline{P}_{\mathrm{t,ref}}}, \tag{33}$$

where $\overline{P}_{\mathrm{t,ref}}$ is the power reference value. In this case, we consider $\overline{P}_{\mathrm{t,ref}}=101\,\mathrm{kW}$. This function is expected to maximize the annual-averaged power available to the turbine, however it should penalize configurations with high surge and pitch motion, as well as regions where parametric resonance is expected.

Table III
GEOMETRICAL CONSTRAINTS CONSIDERED FOR THE GEOMETRY OPTIMIZATION OF THE OWC SPAR BUOY.

| | Constraint | Units |
|---|---|---|
| 1 | $\alpha_{3a}>0.0$ | deg |
| 2 | $\alpha_{3a}<15.0$ | deg |
| 3 | $\alpha_{3e}<15.0$ | deg |
| 4 | $t_{\mathrm{aux}}<t_3$ | m |
| 5 | $l_{2b}>d_2/4$ | m |

Table IV
DESIGN PARAMETERS CONSIDERED FOR THE TURBINE COEFFICIENT AND MASS DISTRIBUTION OPTIMIZATION.

| Parameter | Initial guess | Lower bound | Upper bound |
|---|---|---|---|
| $k_{\mathrm{t}}$ [m s] | 0.0105 | 0.0017 | 0.0595 |
| $c_{\mathrm{m}}$ [-] | 0.10 | 0.00 | 1.00 |

## IV. RESULTS

This section presents the results of three optimizations that consider the same device diameter ($d_1=12\,\mathrm{m}$) and different draft ($l_t=l_1+l_2+l_3=36,48,60\,\mathrm{m}$). Details on the dimensions are shown in Fig. 2. The initial geometry that starts the optimization process was based on the 12 m-diameter and 36 m-draft buoy reported in [5]. For the buoys with $l_t=48,60\,\mathrm{m}$, the dimension $l_{2b}$ was adjusted to match the value of $l_t$. In all cases, $l_1$ was set to 5 m. Table I shows the parameters used in the modelling of the device dynamics. For the computation of the annual-averaged power available to the turbine (see (20)), a wave climate from a location off the western coast of Portugal was considered. This wave climate is characterized by 14 sea states and their spectral distribution is described by a Pierson-Moskowitz spectrum [5].

The main optimization problem (geometry optimization) considered seven variables (design parameters), all dimensions of the device ($l_3,d_3,t_2,t_3,l_{3a},l_{3e},d_2$). Table II shows the seven design parameters and their lower and upper bounds. In order to avoid undesirable geometries, the five inequality constraints presented in Table II were considered. The first three inequalities refer to the angles of the conical surfaces at the bottom section, which were limited to a maximum angle of $15\,\mathrm{deg}$ to avoid flow separation under decelerating flow conditions. The fourth inequality avoids interception between the inner and outer surface of the bottom part, where the auxiliary dimension $t_{\mathrm{aux}}$ represents the minimum length allowed of dimension $t_3$. The fifth inequality guarantees a minimum value for the length of the small thickness tube $l_{2b}$.

The internal optimization problem solves the optimal mass distribution and turbine characteristic. Table IV presents the parameters used in the internal optimization, namely the turbine coefficient $k_{\mathrm{t}}$ and metacentric height coefficient $c_{\mathrm{m}}$. The initial guess, used to start the optimization process, the lower bound and upper

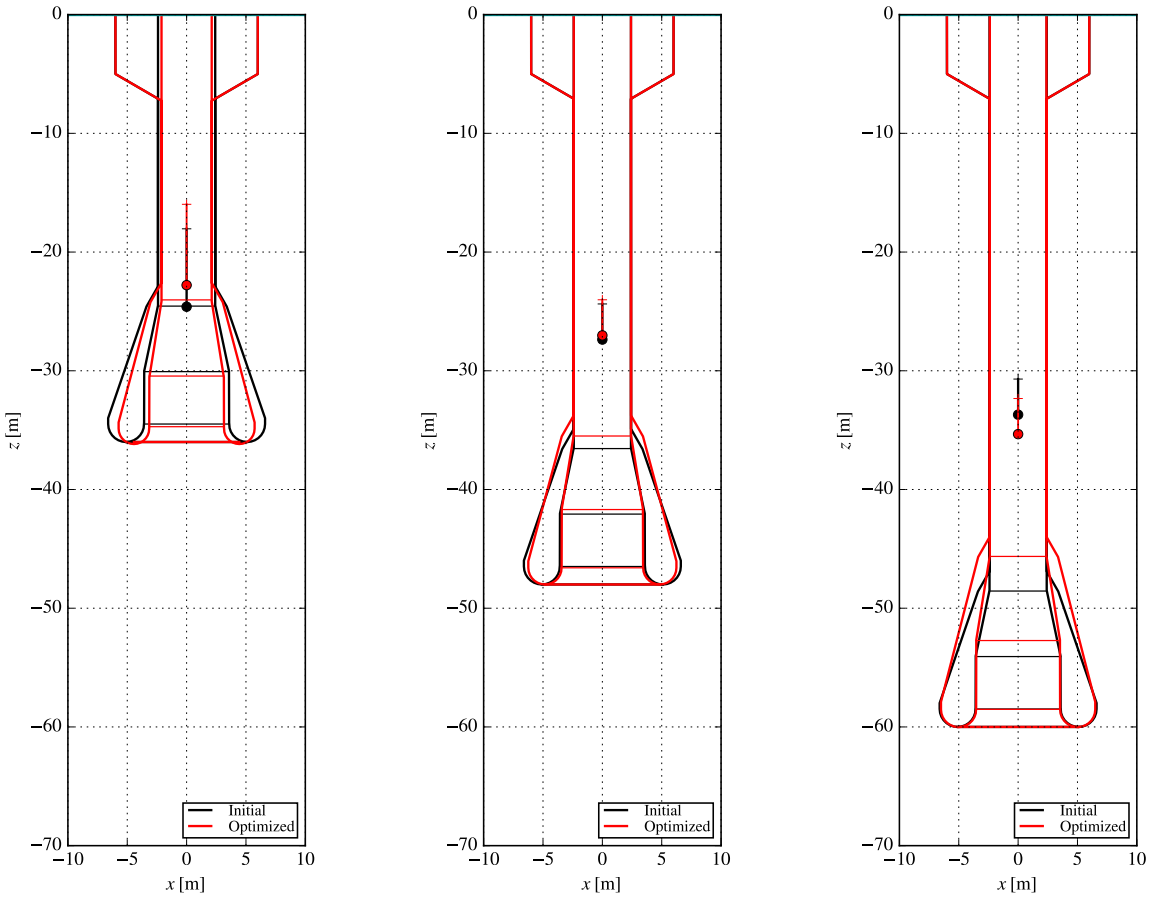


Figure 4. Geometries from the three geometry optimization runs for $l_t = 36, 48, 60$ m. The initial and optimized geometries are presented. The circle represents the position of the centre of mass and the contiguous line represents the metacentric height.

Table V
SUMMARY OF RESULTS FROM THE OPTIMIZATIONS WITH DRAFT EQUAL TO 36, 48 AND 60 M.

| Opt. | Iteration | $l_t$[m] | $m_1$×10$^{-3}$[kg] | $m_{\text{stl}}$×10$^{-3}$[kg] | $T_{n3}$[s] | $T_{n9}$[s] | $T_{n5}$[s] | $\overline{GM}$[m] | $f_{\text{p,PR}}$ | $f_{\text{obj}}$ | $\overline{P}_{\text{t,ann}}$[kW] |
|---|---|---|---|---|---|---|---|---|---|---|---|
| 1 | initial | 36 | 1217.3 | 252.2 | 9.08 | 11.33 | 13.82 | 6.56 | 0.9941 | 0.516 | 53.9 |
| | final | 36 | 1108.5 | 233.4 | 8.24 | 11.31 | 12.93 | 6.81 | 0.9954 | 0.561 | 58.6 |
| 2 | initial | 48 | 1220.1 | 273.4 | 9.13 | 13.22 | 27.26 | 3.00 | 0.9939 | 0.718 | 74.0 |
| | final | 48 | 1215.4 | 273.8 | 8.87 | 13.26 | 27.06 | 3.00 | 0.9940 | 0.728 | 75.0 |
| 3 | initial | 60 | 1222.9 | 294.7 | 9.15 | 14.91 | 36.71 | 3.00 | 0.9999 | 0.786 | 80.3 |
| | final | 60 | 1349.3 | 304.3 | 9.39 | 14.50 | 35.65 | 3.00 | 0.9999 | 0.797 | 81.4 |

bound are presented. In this case, no constraints were applied.

The results of the three optimizations ($l_t = 36, 48, 60$ m), considering the objective function described in (33), are presented in Table V and Fig. 4.

Table V shows results for the each optimized geometry and for each initial geometry (initial iteration). The table presents values of the draft $l_t$ set in the optimization, mass of device $m_1$, mass of the steel structure $m_{\text{stl}}$, buoy's natural heave period $T_{n3}$, OWC's natural heave period $T_{n9}$, buoy's natural pitch period $T_{n5}$, metacentric height $\overline{GM}$, value of penalty function $f_{\text{p,PR}}$, value of objective function $f_{\text{obj}}$ and annual-averaged power $\overline{P}_{\text{t,ann}}$. The difference found between the annual-averaged power values reported in [5] and the ones presented in Table V is related with the application of drag forces in this model.

As shown in Fig. 4, the initial and final geometries are not significantly different. However, by analysing Table V in detail we can find some interesting results by comparing the initial and the final optimization results. For the optimization with $l_t = 36$ m, the device mass ($m_1$) decreases, which is followed by a decrease of the buoy heave natural period $T_{n3}$. For $l_t = 48$ m, $m_1$ and $T_{n3}$ are approximately unchanged. For the case with $l_t = 60$ m, $m_1$ and $T_{n3}$ increase. The mass of steel ($m_{\text{stl}}$) follows the same trend as the device mass ($m_1$).

The pitch natural period shows a relatively low value for the optimization with $l_t = 36$ m ($T_{n5} = 12.93$ s), with a metacentric height value of 6.81 m. The penalty function $f_{\text{p,PR}}$ shows a slight improvement. The parametric resonance effect, which tends to occur around $T_{n5}/2$, in this case should occur at a period below $T_{n3}$ and most usual wave periods (7-12 s). For the cases with $l_t = 48, 60$ m, $T_{n5}$ presents considerably higher values, and therefore $T_{n5}/2$ is located at a period above $T_{n3}$

and $T_{n9}$. The metacentric height $\overline{GM}$ converged to the minimum value.

In all optimizations, the annual-averaged power showed improvements, even though this was not guaranteed at start due to the application of penalty functions in the objective function. The improvements in annual-averaged power were 8.7% ($l_t = 36\,\mathrm{m}$), 1.4% ($l_t = 48\,\mathrm{m}$) and 1.4% ($l_t = 60\,\mathrm{m}$). As observed in [5], these results also show evidence of the high impact that the draft has in the power extraction. Comparing the optimum geometries with $l_t = 36\,\mathrm{m}$ and with $l_t = 60\,\mathrm{m}$, which corresponds to an increase of 66.6% in draft ($l_t$), an increase of 38.9% in power extraction ($\overline{P}_{\mathrm{t,ann}}$), an increase of 21.7% in total mass ($m_1$), and an increase of 30.4% in the mass of steel ($m_{\mathrm{stl}}$) are observed. The longer draft configurations also show less influence from parametric resonance effects.

## V. Conclusions

A new optimization method for designing the shape of the OWC spar buoy device is proposed. The method also optimizes the mass distribution and the turbine coefficient. The converter performance under irregular sea states with several degrees of freedom is modelled in the framework of linear wave theory and small amplitude motions. Drag forces due to viscous effects are considered in the dynamic model. An empirical estimation of the impact of parametric resonance on the power extraction is taken into account in the optimization process. The mass distribution optimization considers that the device consists of a steel structure with constant thickness and the ballast can be placed in two compartments at distinct vertical levels to control the metacentric height.

Three optimizations were carried out for the same buoy diameter and different drafts. Seven design parameters were considered for the geometry optimization. In all cases, the results show improvements in the annual-averaged power available to the turbine, with relative increases between 1.4% and 8.7%. The results indicate that power extraction increases with the draft of the device, at a higher rate than the increase of the total mass and of the mass of steel structure. Longer drafts also seem to have the advantage of being less prone to parametric resonance.

## Acknowledgement

This work was partially supported by the Portuguese Foundation for Science and Technology (FCT), through IDMEC, under LAETA, project UID/EMS/50022/2019 and by the European Commission's Horizon 2020 program, project WETFEET, under grant No. 641334. R. P. F. Gomes was supported by post-doctoral fellowship SFRH/BPD/93209/2013 from FCT. J. C. C. Henriques was supported by FCT researcher grant No. IF/01457/2014.

## References

[1] A. Clément, A. Babarit, J. C. Gilloteaux, C. Josset, and G. Duclos, "The SEAREV wave energy converter," in *Proc. 6$^{\mathrm{th}}$ European Wave and Tidal Energy Conference*, Glasgow, UK, 2005.

[2] J. Cordonnier, F. Gorintin, A. De Cagny, A. H. Clément, and A. Babarit, "SEAREV: Case study of the development of a wave energy converter," *Renewable Energy*, vol. 80, pp. 40–52, 2015.

[3] A. P. McCabe, "Constrained optimization of the shape of a wave energy collector by genetic algorithm," *Renewable Energy*, vol. 51, pp. 274–284, 2013.

[4] R. P. F. Gomes, J. C. C. Henriques, L. M. C. Gato, and A. F. O. Falcão, "IPS 2-body wave energy converter: Acceleration tube optimization," *International Journal of Offshore and Polar Engineering*, vol. 20, no. 4, pp. 247–255, 2010.

[5] ——, "Hydrodynamic optimization of an axisymmetric floating oscillating water column for wave energy conversion," *Renewable Energy*, vol. 44, pp. 328 – 339, 2012.

[6] S. Esmaeilzadeh and M.-R. Alam, "Shape optimization of wave energy converters for broadband directional incident waves," *Ocean Engineering*, vol. 174, pp. 186–200, 2019.

[7] S. Ribeiro e Silva, R. P. F. Gomes, and A. F. O. Falcão, "Hydrodynamic optimization of the UGEN: Wave energy converter with U-shaped interior oscillating water column," *International Journal of Marine Energy*, vol. 15, pp. 112–126, 2016.

[8] Y. Masuda, "An experience of wave power generator through tests and improvment," in *Hydrodynamics of Ocean Wave Energy Utilization Symposium*, D. V. Evans and A. F. de O. Falcão, Eds., Lisbon, Portugal, 1985.

[9] M. E. McCormick, "Analysis of a wave energy conversion buoy," *Journal of Hydronautics*, vol. 8, no. 3, pp. 77–82, 1974.

[10] T. J. T. Whittaker and F. A. McPeake, "Design optimization of axi-symmetric tail tube buoys," in *Hydrodynamics of Ocean Wave Energy Utilization Symposium*, D. V. Evans and A. F. de O. Falcão, Eds., Lisbon, Portugal, 1985.

[11] M. A. Alves, I. R. Costa, A. J. N. A. Sarmento, and J. F. Chozas, "Performance evaluation of an axysimmetric floating OWC," in *Proc. 20$^{\mathrm{th}}$ International Offshore and Polar Engineering Conference*, Beijing, China, 2010.

[12] R. P. F. Gomes, J. C. C. Henriques, L. M. C. Gato, and A. F. O. Falcão, "Wave power extraction of a heaving floating oscillating water column in a wave channel," *Renewable Energy*, vol. 99, pp. 1262–1275, 2016.

[13] R. P. F. Gomes, J. D. C. Malvar Ferreira, S. Ribeiro e Silva, J. C. C. Henriques, L. M. C. Gato, and A. F. O. Falcão, "An experimental study on the reduction of the dynamic instability in the oscillating water column spar buoy," in *Proc. 12$^{\mathrm{th}}$ European Wave and Tidal Energy Conference*, Cork, Ireland, 2017.

[14] K. Tarrant and C. Meskell, "Investigation on parametrically excited motions of point absorbers in regular waves," *Ocean Engineering*, vol. 111, pp. 67–81, 2016.

[15] G. Giorgi and J. V. Ringwood, "Articulating parametric resonance for an OWC spar buoy in regular and irregular waves," *Journal of Ocean Engineering and Marine Energy*, vol. 4, pp. 311–322, 2018.

[16] A. J. N. A. Sarmento and A. F. de O. Falcão, "Wave generation by an oscillating surface-pressure and its application inwave energy extraction," *Journal of Fluid Mechanics*, vol. 150, pp. 481–499, 1985.

[17] A. F. de O. Falcão and P. A. P. Justino, "OWC wave energy devices with air flow control," *Ocean Engineering*, vol. 26, no. 12, pp. 1275–1295, 1999.

[18] C.-H. Lee and J. Newman, "Computation of wave effects using the panel method," in *Numerical Models in Fluid-Structure Interaction*, S. Chakrabarti, Ed. Southampton, United Kingdom: WIT Press, 2005.

[19] A. F. de O. Falcão and R. J. A. Rodrigues, "Stochastic modelling of OWC wave power plant performance," *Applied Ocean Research*, vol. 24, no. 2, pp. 59–71, 2002.

[20] T. Sarpkaya and M. Isaacson, *Mechanics of wave forces on offshore structures*. New York, USA: Van Nostrand Reinhold, 1981.

[21] S. K. Chakrabarti, *Offshore structure modeling*. Singapore: World Scientific, 1994.

[22] R. G. Dean and R. A. Dalrymple, *Water Wave Mechanics for Engineers and Scientists*. World Scientific, 1984.

[23] M. J. D. Powell, "A direct search optimization method that models the objective and constraint functions by linear interpolation," in *Advances in Optimization and Numerical Analysis*, S. Gomez and J. P. Hennart, Eds. Dordrecht, Netherlands: Kluwer Academic, 1994, pp. 51–67.

[24] J. E. Kerwin, "Notes on rolling in longitudinal waves," *International Shipbuilding Progress*, vol. 2, no. 16, pp. 597–614, 1955.

[25] D. W. Jordan and P. Smith, *Nonlinear Ordinary Differential Equations: An introduction for Scientists and Engineers*, 4th ed. New York, USA: Oxford University Press, 2007.